Proc. Natl. Acad. Sci. USA
Vol. 92, pp. 11427–11433, December 1995
Colloquium Paper

This paper was presented at a colloquium entitled "Quasars and Active Galactic Nuclei: High Resolution Radio Imaging," organized by a committee chaired by Marshall Cohen and Kenneth Kellermann, held March 24 and 25, 1995, at the National Academy of Sciences Beckman Center, Irvine, CA.

Probing active galactic nuclei with H_2O megamasers

JAMES MORAN*, LINCOLN GREENHILL*, JAMES HERRNSTEIN*, PHILIP DIAMOND†, MAKOTO MIYOSHI‡, NAOMASA NAKAI§, AND MAKOTO INOUE§

*Harvard–Smithsonian Center for Astrophysics, Mail Stop 42, 60 Garden Street, Cambridge, MA 02138; †National Radio Astronomy Observatory, P.O. Box O, Socorro, NM 87801; ‡Mizusawa Astrogeodynamics Observatory, National Astronomical Observatory, 2-12 Hoshigaoka, Mizusawa, Iwate 023, Japan; and §Nobeyama Radio Observatory, National Astronomical Observatory, Minamisaku, Minamimaki, Nagano, 384-13, Japan

ABSTRACT **We describe the characteristics of the rapidly rotating molecular disk in the nucleus of the mildly active galaxy NGC4258. The morphology and kinematics of the disk are delineated by the point-like water-vapor emission sources at 1.35-cm wavelength. High angular resolution [200 μas where as is arcsec, corresponding to 0.006 parsec (pc) at 6.4 million pc] and high spectral resolution (0.2 km·s^{-1} or $\nu/\Delta\nu = 1.4 \times 10^6$) with the Very-Long-Baseline Array allow precise definition of the disk. The disk is very thin, but slightly warped, and is viewed nearly edge-on. The masers show that the disk is in nearly perfect Keplerian rotation within the observable range of radii of 0.13–0.26 pc. The approximately random deviations from the Keplerian rotation curve among the high-velocity masers are ≈3.5 km·s^{-1} (rms). These deviations may be due to the masers lying off the midline by about ±4° or variations in the inclination of the disk by ±4°. Lack of systematic deviations indicates that the disk has a mass of $<4 \times 10^6$ solar mass ($M_\odot$). The gravitational binding mass is $3.5 \times 10^7 M_\odot$, which must lie within the inner radius of the disk and requires that the mass density be $>4 \times 10^9 M_\odot \cdot pc^{-3}$. If the central mass were in the form of a star cluster with a density distribution such as a Plummer model, then the central mass density would be $4 \times 10^{12} M_\odot \cdot pc^{-3}$. The lifetime of such a cluster would be short with respect to the age of the galaxy [Maoz, E. (1995) *Astrophys. J. Lett.* 447, L91–L94]. Therefore, the central mass may be a black hole. The disk as traced by the systemic velocity features is unresolved in the vertical direction, indicating that its scale height is <0.0003 pc (hence the ratio of thickness to radius, H/R, is <0.0025). For a disk in hydrostatic equilibrium the quadrature sum of the sound speed and Alfven velocity is <2.5 km·s^{-1}, so that the temperature of the disk must be <1000 K and the toroidal magnetic field component must be <250 mG. If the molecular mass density in the disk is 10^{10} cm^{-3}, then the disk mass is $\approx 10^4 M_\odot$, and the disk is marginally stable as defined by the Toomre stability parameter Q ($Q = 6$ at the inner edge and 1 at the outer edge). The inward drift velocity is predicted to be <0.007 km·s^{-1}, for a viscosity parameter of 0.1, and the accretion rate is $<7 \times 10^{-5} M_\odot \cdot yr^{-1}$. At this value the accretion would be sufficient to power the nuclear x-ray source of 4×10^{40} ergs^{-1} (1 erg = 0.1 μJ). The volume of individual maser components may be as large as 10^{46} cm^3, based on the velocity gradients, which is sufficient to supply the observed luminosity. The pump power undoubtedly comes from the nucleus, perhaps in the form of x-rays. The warp may allow the pump radiation to penetrate the disk obliquely [Neufeld, D. A. & Maloney, P. R. (1995) *Astrophys. J. Lett.* 447, L17–L19]. A total of 15 H_2O megamasers have been identified out of >250 galaxies searched. Galaxy NGC4258 may be the only case where conditions are optimal to reveal a well-defined nuclear disk. Future measurement of proper motions and accelerations for NGC4258 will yield an accurate distance and a more precise definition of the dynamics of the disk.**

The association between powerful water vapor masers and active galactic nuclei (AGN) has been known for ≈15 years. The first examples were found by dos Santos and Lepine (1) in galaxy NGC4945, by Gardner and Whiteoak (2) in the Circinus galaxy, by Henkel *et al.* (3) and Haschick and Baan (4) in galaxy NGC3079, and by Claussen *et al.* (5) in galaxies NGC1068 and NGC4258. dos Santos and Lepine (1) followed the lead of Churchwell *et al.* (6), who discovered the first extragalactic H_2O maser in M33, which lies in its spiral arms and is similar in apparent luminosity to masers in galactic star-forming regions. Preliminary very-long-baseline radio interferometry (VLBI) observations of NGC3079 and NGC4258 by Haschick *et al.* (7) and Claussen *et al.* (8), respectively, showed that the strongest spectral features arose from extremely compact regions [≤0.1 parsec (pc)]. From these studies it became clear that masers in the nuclei of galaxies were a fundamentally different phenomenon from those in the galaxy and in the spiral arms of nearby galaxies. For example, while some nuclear maser sources had about the same linear extents as galactic masers, the apparent luminosities were orders of magnitude larger—hence the designation "megamaser."

Recent VLBI observations by Miyoshi *et al.* (9) have shown that in NGC4258, the maser emission arises from a remarkably well-defined, rapidly rotating, molecular disk, which is probably within ≈0.25 pc of the nucleus of the galaxy and whose parameters can be estimated to high precision. In this paper we describe some details of this work that are not covered in the original paper. The basic analysis of the data will not be repeated here. We also discuss the prospect of finding other examples of such compact molecular disks.

Historical Background

The megamaser in galaxy NGC4258 was discovered by Claussen *et al.* (5) during their survey of bright IRAS galaxies. They discovered four masers in the 73 nuclei they searched. Claussen and Lo (10) suggested that the masers, especially the ones in NGC1068 and NGC4258, might be associated with molecular tori, as envisioned by Antonucci and Miller (11) and discussed the veracity of such a model. Before then, H_2O megamasers were generally thought to be associated with regions of star formation, by analogy with masers in our galaxy.

The publication costs of this article were defrayed in part by page charge payment. This article must therefore be hereby marked "*advertisement*" in accordance with 18 U.S.C. §1734 solely to indicate this fact.

Abbreviations: pc, parsec; Mpc, million parsec; VLBI, very-long-baseline radio interferometry; μas and mas, microarcsec and milliarcsec, respectively; Jy, Jansky; $M_\odot$, solar mass.

A quick look at data from a VLBI experiment in 1984 on the maser emission near the systemic velocity of the galaxy NGC4258 showed that the features had separations on the order of 0.1 milliarcsec (mas) (8). Reanalysis of this data by Greenhill and Jiang revealed an interesting linear correlation between velocity and position. This data provided direct evidence that the maser emission arose from a rotating disk (12). Although the spread in position was only about one beamwidth, the masers were well separated in velocity, and, because they were point-like, their positions could be determined to a small fraction of the beamwidth.

In the meantime Nakai *et al.* (13) coupled eight new acousto-optical spectrometers on the Nobeyama Radio Observatory (NRO) 45-m telescope to form a contiguous spectrometer of 16,000 channels. They observed the water maser in NGC4258 and made the astonishing discovery that, in addition to the spectral features near the systemic velocity, there were groups of features displaced by 1000 km·s^{-1} on either side of them (Fig. 1). Their brief, single baseline VLBI observation within Japan demonstrated that all the features were coincident to within 50 mas. They argued that the high-velocity lines were unlikely to be lines of other molecular species, and they suggested three interpretations for the high-velocity emission: (*i*) a nonkinematic origin—Raman scattering in an ionized region with a plasma frequency of ≈75 MHz (see also ref. 15); (*ii*) a bipolar outflow; or (*iii*) a disk, where the high-velocity emission arises along a diameter perpendicular to the line of sight.

In parallel to the VLBI observations and the work of Nakai *et al.* (13), Haschick *et al.* (16) had acquired a large body of time-variation data with the Haystack 37-m telescope, as had another group with the Effelsberg 100-m telescope (17). Together, the data, which covered the period from 1984 to 1994, showed a secular drift among all the strong maser components near the systemic velocity of ≈9 km·s^{-1}·yr^{-1}. Features diminished in intensity at high velocity and new features appeared at low velocity, so that the centroid velocity remained constant. The Effelsberg data also showed that the high-velocity emission did not drift by >1 km·s^{-1}·yr^{-1} over 1993–1994. Watson and Wallin (14) made the important contribution [based on a review of the Haystack and Effelsberg spectroscopy (17, 18), the VLBI imaging of the systemic emission (12), and the wideband spectroscopy at NRO (13)] that the high-velocity features could arise along the midline of a rotating edge-on disk, and that the drift rate of the systemic features could be attributed to the centripetal acceleration. During International Astronomical Union Colloquium 140 in Hakone, Japan, in October 1992 a collaboration between United States and Japanese astronomers was formed to perform more definitive observations with the Very-Long-Baseline Array (VLBA), which was not fully operational at the time. Data were taken in April 1994. The first images of the high-velocity features were glimpsed in October 1994. One of three results had been expected: (*i*) the high-velocity features would be coincident with the systemic features, supporting the hypothesis of Raman scattering; (*ii*) the high-velocity features would be placed off the plane of the previously inferred disk (i.e., outflow); or (*iii*) the high-velocity features would be found to lie in the plane of the disk, and on the position–velocity plot at two points consistent with the trend established by the systemic features. In fact, what we found was that the high-velocity features were separated from the systemic features, in the plane of the disk, and most striking, with a position–velocity distribution that traced a nearly perfect Keplerian curve. This characteristic confirmed the basic features of the disk model but led to the puzzling realization that while the systemic emission arose from a thin annular ring, the high-velocity emission arose from a wide one, with an outer radius about twice the inner radius.

VLBI Imaging

In the observations described by Miyoshi *et al.* (9) the visibility data in each spectral channel were referenced to the phase of a reference feature. Then the image in each spectral (velocity) channel was fit to multiple Gaussian profiles. The rms error in relative position of each channel was assigned according to the formula

$$\sigma_{x,y} = \frac{1}{2}\frac{\psi_{x,y}}{SNR}, \qquad [1]$$

where σ_x and σ_y are the errors in right ascension and declination, respectively, *SNR* is the signal-to-noise ratio (feature amplitude/rms noise in image), and ψ_x and ψ_y are the angular resolutions in the right ascension and declination directions,

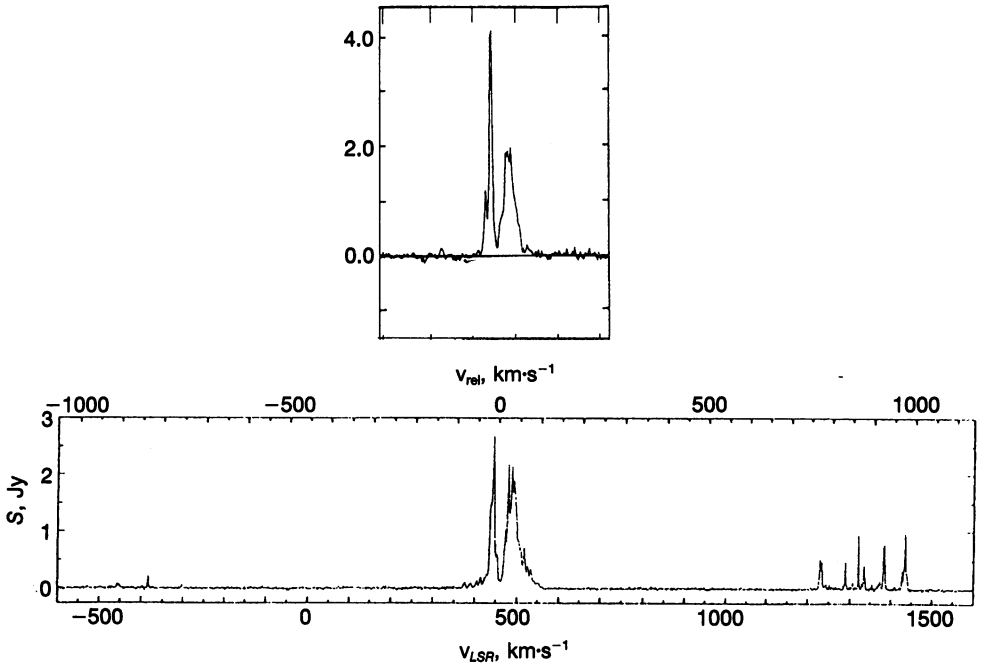

FIG. 1. Spectra of the H_2O maser emission from the nucleus of NGC4258. (*Upper*) Spectrum of emission close to the systemic velocity of the galaxy obtained by Claussen *et al.* (5) with a 1024-channel spectrometer in 1982. (*Lower*) Spectrum obtained by Nakai *et al.* (13) using a 16,000-channel spectrometer in 1992. Note that the absence of emission near the system velocity of ≈476 km·s^{-1} may be a permanent characteristic of the spectrum. Watson and Wallin (14) propose that a layer of nonmasing water vapor interior to the disk absorbs the continuum radiation from the nucleus at the systemic velocity, thereby inhibiting maser emission at that velocity. LSR, Local Standard of Rest.

respectively. Systematic errors among the systemic-velocity features are expected to be very small, <1 microarcsec (μas), because the field of view and delay errors are small (19). Hence, the systematic errors are negligible for *SNR* below ≈300, and no greater *SNR* was achieved. For the high velocity features the uncertainty in the absolute position of the reference feature causes a systematic error of $\theta_e = \Delta\theta\Delta\nu/\nu$, where $\Delta\theta$ is the vector offset between the true reference position and the position used in processing, $\Delta\nu$ is the frequency offset from the reference frequency, and ν is the frequency. This error can be significant but is constant in time and will not affect proper motion estimates. The current accuracy of the absolute position is about 0.04 arcsec (12), which means that the differential systematic errors are <40 μas. The proper assignment of error values is important for the evaluation of systematic deviations from the model fits described below.

In the course of the analysis the velocities were corrected for relativistic effects that can be described by the formula

$$v_z = v_a + \frac{v_a^2}{2c} - \frac{v_t^2}{2c} - \frac{GM}{Rc}, \quad [2]$$

where v_z is the true line-of-sight velocity, v_a is the observed line-of-sight velocity [radio definition of Doppler shift, i.e., $v_a = c(\nu_0 - \nu)/\nu_0$, where ν_0 is the transition frequency, ν is the observation frequency, and c is the speed of light], v_t is the transverse velocity, and in the last term, which describes the gravitational red-shift, G is the gravitational constant, M is the mass of the central object, and R is the radial distance from the central mass. These relativistic effects are small, but noticeable: the transverse Doppler shift is ≈2 km·s^{-1}, and the gravitational shift is ≈4 km·s^{-1}.

The shift in position of the masers because of gravitational lensing of the high-velocity features is small because the emission originates near the deflector (20); that is, the bending is given by

$$\phi = \frac{2GM}{c^2R}\left(\frac{R}{D}\right), \quad [3]$$

where D is distance to the galaxy. The term in parentheses, the "lever arm," reduces the deflection to a value

$$\phi = \frac{R_s}{D}, \quad [4]$$

which is independent of separation from the central object, where R_s is the Schwarzschild radius. Hence, although $2GM/c^2R$ is ≈11 arcsec, ϕ is only ≈0.1 μas.

In actual practice the data have been analyzed globally. However, it is instructive to discuss separately individual aspects of the data that most strongly constrain particular physical parameters. For example, from inspection of the image data (figure 2 in ref. 9) it can be determined that the disk is nearly edge-on but tipped slightly to the south at an inclination of 97° and has a position angle of 87°.

The Keplerian Position–Velocity Curve

The positions and velocities of the features are accurately fit by a Keplerian curve, given by

$$v_z - v_o = \sqrt{\frac{GM}{R}}\sin\theta, \quad [5]$$

where θ is the angle in the plane of the disk between the direction to the maser and to the observer and v_o is the systemic velocity. A position–velocity diagram for the high-velocity features is shown in Fig. 2. Because the dependence of velocity on position closely follows a classic Keplerian curve, it is clear

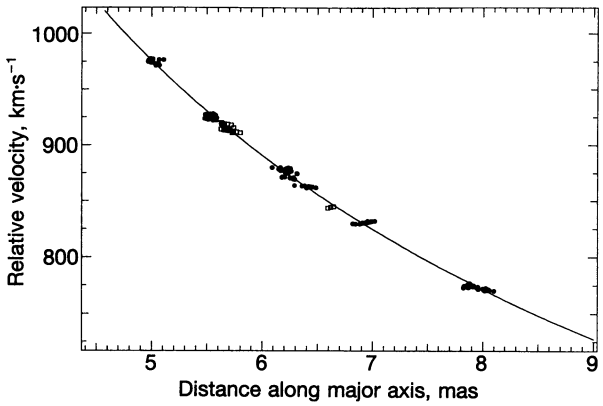

FIG. 2. Keplerian rotation curve displayed by high-velocity maser features. Velocities and radii are with respect to the systemic velocity of the galaxy (476 km·s^{-1} Local Standard of Rest) and position of the central massive object, respectively. The magnitude of the velocities is shown so that the redshifted (●) and blueshifted (□) emission are overlaid. The velocity range of the emission has been roughly the same as shown here since its discovery.

that θ is nearly constant. From considerations discussed below, including the fact that the high-velocity features show no centripetal acceleration (17), it is most likely that $\theta = 90°$; that is, the masers lie on a midline (diameter) through the disk, perpendicular to the line of sight. Why we should observe such a clean Keplerian curve is not totally obvious. However, we accept it as a fact and reject more complex models where the angular dependence of θ exactly compensates some other radial dependence so as to mimic a Keplerian curve. With sin $\theta = 1$ we used Eq. **5** to solve for four parameters: M, the central mass; x_o and y_o, the central coordinates of the disk (origin of R); and v_o, the systemic line-of-sight velocity of the disk (which presumably is the systemic velocity of the galaxy). These values are 3.5 × 10^7 solar mass ($M_\odot$) [more precisely, the mass estimate is 3.5 × 10^7 (6.4 Mpc/D)(sin 97°/sin i)(1/sin θ)], −0.19 mas, 0.60 mas, and 476 km·s^{-1}, with respect to the Local Standard of Rest (LSR). The value of the reduced χ^2 is ≈3. This value can be reduced to unity by adding a 1 − σ position error, σ_r, of 40 μas to the measurement errors. Part of this error is probably due to the systematic effect of the error in position of the reference feature, as described above. The added error can be converted to an equivalent velocity error by the relation, derivable from Eq. **5**, given by

$$\sigma_v = \frac{1}{2}\frac{v_z}{R}\sigma_r, \quad [6]$$

which yields for the midradius of the disk a value of 3.5 km·s^{-1}. There could be several origins for the increased scatter. A spread in angle from the midline of ±4° among the high-velocity masers or a variation in the inclination angle of various annular components of the disk of about ±4°. Note that there are systematic trends in the velocity residuals across individual maser features.

We can replace the central point mass with a mass model that includes the mass of the disk, such as

$$M_T = M + \pi\Sigma R^2, \quad [7]$$

where Σ is the vertical column density of material in the disk. This model does not reduce the value of χ^2. We placed a 3σ limit on the disk mass of 4 × 10^6 $M_\odot$, for a radius-independent Σ.

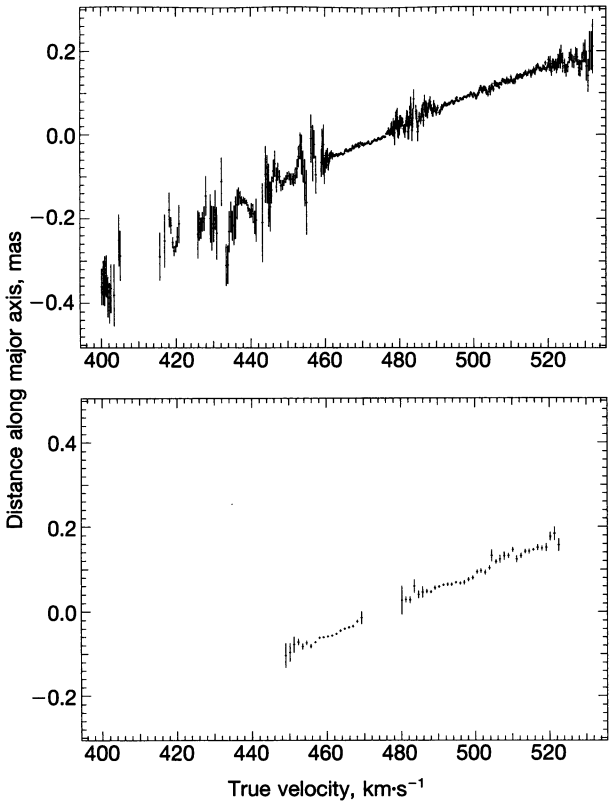

FIG. 3. Position–velocity diagrams for the maser emission that is close to the systemic velocity of the galaxy. The observation in 1994 (*Upper*) was sensitive to emission over a wider range of velocity than the observation in 1984 (*Lower*). Emission is known to occur at velocities as high as 580 km·s^{-1}, although neither experiment was sensitive to it. The velocity axis has been corrected for relativistic effects according to Eq. **2**.

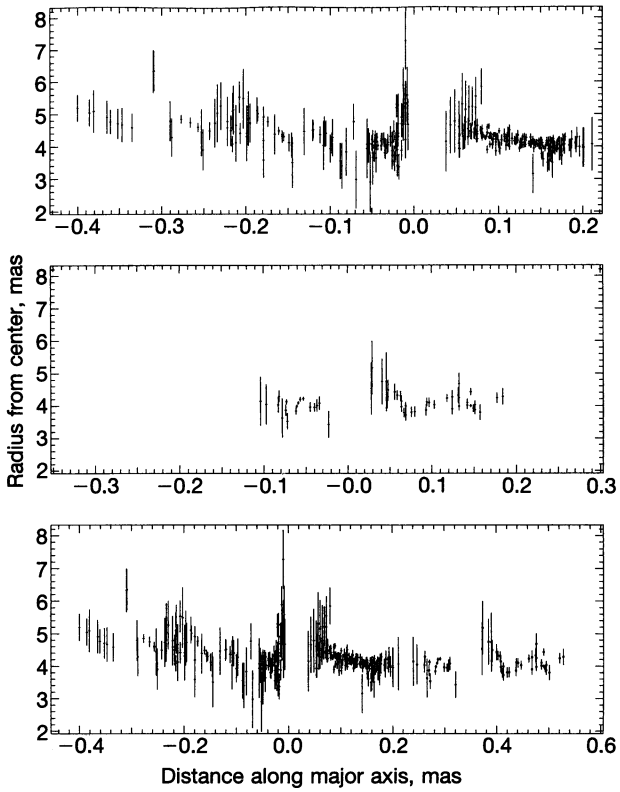

FIG. 4. Estimated radii of the systemic maser features from the central object as a function of projected position in the molecular disk (i.e., impact parameter) for 1994 (*Top*) and for 1984 (*Middle*). The systemic maser features are known to have drifted in velocity by ≈9 km·s^{-1}·yr^{-1} from 1984 to 1994. (*Bottom*) Data from both epochs. Individual maser features probably correspond to distinct clumps or cloudlets within the molecular disk. Velocities of the features from the earlier observation have been shifted in velocity to account for drift over 10 years. Unfortunately, there were no features detected in both experiments.

Disk Geometry

We turn our attention to the masers near the systemic velocity. The positions of these masers change linearly with line-of-sight velocity. Fig. 3 shows the data for the VLBI observations in 1984 and 1994. Because $\sin\theta = (r - r_o)/R$, where $r - r_o$ is the projected radius (i.e., impact parameter), then from Eq. **5** it is clear that all of these masers must have nearly the same radii. We can invert Eq. **5** and find the radius of each maser feature from the relation

$$R = (GM)^{1/3}\left[\frac{(r - r_o)}{(v_z - v_o)}\right]^{2/3}. \qquad [8]$$

The error in this estimate of the radius is given by

$$\sigma_R = \frac{2}{3}R\left[\left(\frac{\sigma_r}{r}\right)^2 + \frac{\sigma_{v_o}^2}{(v_z - v_o)^2}\right]^{1/2}, \qquad [9]$$

where σ_{v_o} is the velocity error. The estimated radii are shown in Fig. 4 for both sets of observations. The radius of the masers changes slightly with position, but the radial spread is typically only 0.1 mas or 0.005 pc. Note that in Fig. 4 *Bottom*, the projected radial position is given for epoch April 1994. Hence, some of the emission seen in 1984 showed us a part of the disk that by April 1994 had already rotated out of view.

We have also examined the distribution of masers in the systemic group in the direction perpendicular to the major axis of the disk. These positions are shown in Fig. 5. The reduced χ^2 is close to unity (0.97) for the model in which all the features are in the plane of the disk. Hence, the vertical thickness of the disk, H, is <0.01 mas or 0.0003 pc, which is a more stringent limit than that reported by Miyoshi *et al.* (9). Thus, $H/R \leq 0.0025$. The disk is probably close to hydrostatic equilibrium (21)—that is,

$$\frac{H}{R} = \frac{c_s}{v_\phi}, \qquad [10]$$

where c_s is the sound speed and v_ϕ is the Keplerian rotational velocity. We obtain $c_s < 2.5$ km·s^{-1} for $H/R < 0.0025$. Hence, because in a neutral molecular cloud, $c_s = 0.08\sqrt{T}$, where T is the gas temperature, we obtain $T < 1000$ K. Similarly, if the vertical pressure is provided by magnetic pressure than c_s in Eq. **10** is replaced by v_A, the Alfvén speed. Because $v_A = B/\sqrt{8\pi\rho}$, where B is the magnetic field strength parallel to the disk and ρ is the gas density, then for a molecular density of 10^{10} cm^{-3}, the toroidal magnetic field must be <250 mG.

The stability of the molecular disk can be estimated from the Toomre stability parameter (22),

$$Q = \frac{c_s\Omega}{\pi G\Sigma}, \qquad [11]$$

where Ω is the angular rotation speed. A disk is stable for $Q \gtrsim 1$. Because $\Omega = v_\phi/R$, $\Sigma = 2\rho H$, $c_s = v_\phi H/R$, and $v_\phi^2 = GM/R$, we obtain

$$Q = \frac{M}{\pi R^3\rho} = \frac{M}{M_D^*}\left(\frac{2H}{R}\right), \qquad [12]$$

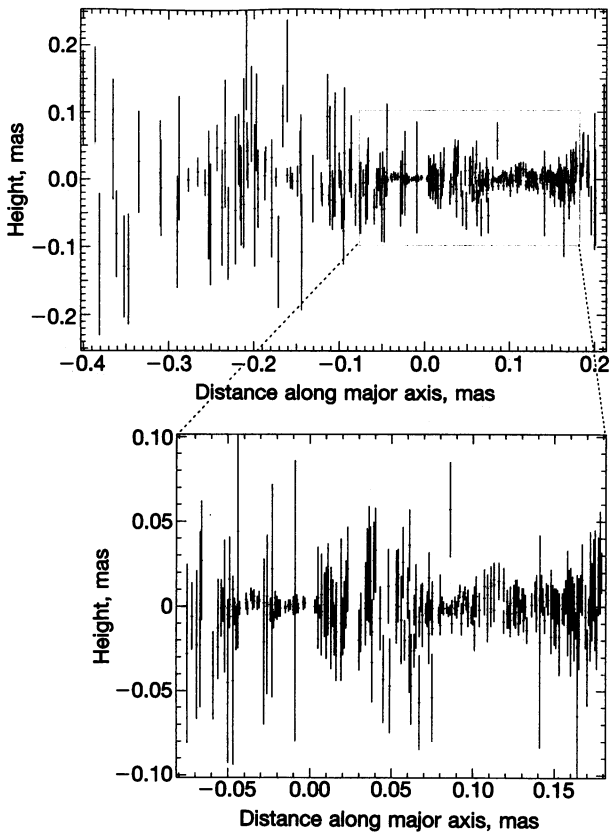

FIG. 5. Estimated height of systemic maser features above or below the plane of the disk in 1994. Thickness of the disk is unresolved by these observations. Errors bars represent 1σ uncertainties in position estimates.

where M_D^* is the mass of the disk interior to R. For a molecular density of 10^{10} cm^{-3} (the maximum allowed to avoid quenching the maser action), $\rho = 3.2 \times 10^{-14}$ g·cm^{-3} and $\Sigma = 56$ g·cm^{-2}, we obtain $Q = 6$ at the inner edge of the disk and $Q = 1$ at the outer edge. Hence, the disk appears to be only marginally stable, especially at its outer edge. Perhaps this explains the absence of maser emission beyond the observed outer radius. The disk stability is discussed further by Maoz (23), who suggests that the regular spacing among the high velocity maser features may indicate the presence of spiral structure.

We can estimate the accretion rate from our data (see also ref. 24). From the continuity equation the accretion rate is

$$\dot{M} = 2\pi R \Sigma v_R , \qquad [13]$$

where v_R is the radial infall drift velocity. The observational limit on the radial velocity is $v_R \lesssim 10$ km·s^{-1} (based on a comparison of optical and radio systemic velocities). This gives a limit on the mass accretion rate of about $1\ M_\odot$·yr^{-1}. From the theory of a stable thin disk (21), $v_R = \alpha v_\phi (H/R)^2$, where α is the viscosity parameter. For $\alpha = 0.1$, $H/R < 0.0025$ we obtain $v_R < 0.0007$ km·s^{-1}, and $\dot{M} = 7 \times 10^{-5}\ M_\odot$·yr^{-1}. Note that the characteristic lifetime of the disk, $M_D/\dot{M} = R^3/(2H^2 v_\phi \alpha) = 10^8$ yr. This is a lower limit. If we take this value as the mass accretion rate and convert it to luminosity with an efficiency of 10%, of which 10% appears as x-ray emission, then it could power an x-ray source of 5×10^{40} erg s^{-1}. The observed x-ray luminosity is 4×10^{40} erg·s^{-1} (25).

A Massive Black Hole?

The high enclosed mass that is inferred from the Keplerian rotation curve (Fig. 2) and the exceptionally small inner radius of the region populated by masers imply a central mass density $>4 \times 10^9\ M_\odot$·pc^{-3}. The greatest known densities for galactic globular clusters are $\approx 10^5\ M_\odot$·pc^{-3}. Whatever binds the masing disk has a very high mass density by the standards of stellar clusters (actually only 3×10^{-13}g·cm^{-3}). The small deviations of the maser features from a Keplerian curve, $\lesssim 3$ km·s^{-1}, limit the number of cluster members that could lie between the inner and outer radii of the masing disk. Maoz (26) adopted a Plummer cluster density model to show that >99% of the cluster mass must lie within the inner radius. Furthermore, within the core radius, the mass density would be $\gtrsim 4.5 \times 10^{12}\ M_\odot$·pc^{-3}. He calculated that if the cluster consisted mainly of stars of mass $>0.03\ M_\odot$, then it would evaporate on a time scale short with respect to the age of the galaxy. On the other hand, if it consisted mainly of objects with mass $<0.03\ M_\odot$, then the cluster would be disrupted by physical collisions on a similiarly short time scale. Hence, the high precision of the Keplerian rotation curve of the high-velocity maser features strongly suggests that the central mass is not a stellar cluster, but rather a supermassive black hole.

The case for massive black holes in other galaxies, including our own, is reviewed by Kormendy and Richstone (27). The limit on the mass density for the object in NGC4258 is much greater than any of the other massive black hole candidates,

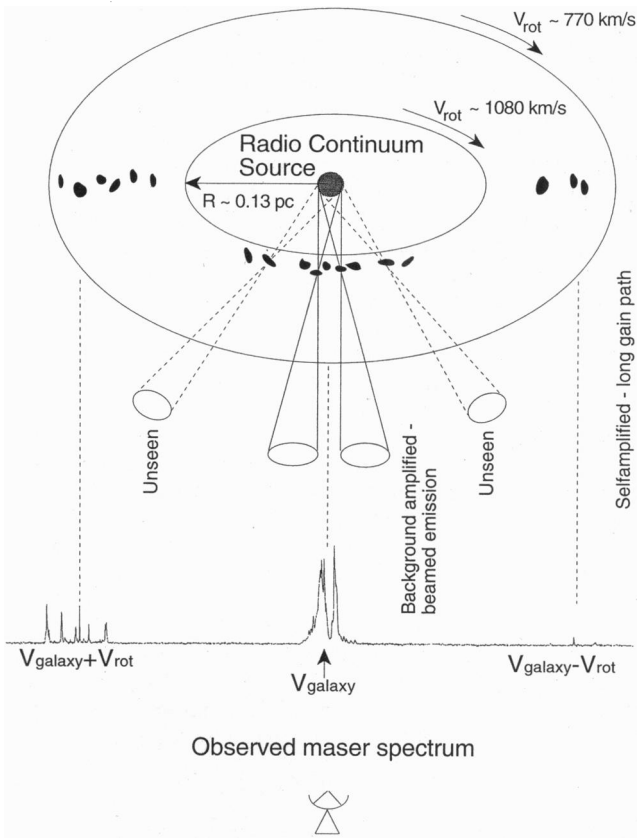

FIG. 6. Cartoon of the maser geometry for a nearly edge-on disk. The view is from slightly above the plane containing the disk and the Earth. The masing region occupies an annulus, with a fractional radial thickness of 0.5, that probably lies within a more extensive dusty torus. Masers in the systemic-velocity group become visible to us when they pass in front of the continuum source, which they amplify, and whose diameter may be inferred from the angular extent of the maser features. However, the high-velocity features do not amplify a background source, relying instead on long velocity-coherent gain paths through the disk. The emission that we see is beamed anisotropically. However, the disk structure is apparent, presumably, to all observers for whom it is nearly edge-on. V_{rot}, disk rotation velocity; V_{galaxy}, galaxy velocity.

primarily because of the high angular resolution of the VLBI observations. Note that the Schwarzschild radius for the object in NGC4258 is 1×10^{13} cm, so that the inner edge of the maser disk lies at a distance of 40,000 R_s from the putative black hole. Hence, the direct observational effects are small. Ruffini and Stella (28) calculated the expected appearance of a maser close to the Schwarzschild radius.

Maser Amplification

The masers actually trace only a small part of the circumnuclear disk, as depicted in Fig. 6. Maser emission may disappear at radii <4 mas and >8 mas because of unfavorable excitation conditions (24). The appearance of masers along the line of sight to the nucleus and along the midline of the disk are undoubtedly related to the fact that in these directions the gradient of the line-of-sight velocity is zero, and hence, these directions support long pathlengths for coherent amplification. The distribution of high-velocity features along the midline at radii of 4–8 mas and the confinement of the systemic features to a narrow annulus are hard to understand. A plausible explanation can be found in the fact that the disk is slightly warped. (Note that the physical origin of the warp is not known. However, mechanisms proposed for warps in galactic black hole candidates may be relevant—e.g., see ref. 29.) If we assume, as is plausible from the image (see figure 2 in ref. 9), that the maximum warp is along the midline and the line of nodes points nearly toward the earth, then the pump energy from the nucleus, perhaps in the form of x-rays that heat the molecular gas (see ref. 24), can illuminate the disk obliquely and power the high-velocity masers over a wide range of radii. Along the line of sight to the systemic features the disk is much less warped, and the radiation does not penetrate as far into the disk. The radial depth over which maser emission might occur for these components is estimated to be ≈0.001 pc by Neufeld *et al.* (30) for relevant physical conditions, which is roughly consistent with the observations (see Fig. 4). This would explain the narrow annular ring of maser emission close to the systemic velocity of the galaxy.

Although the individual maser features are unresolved, we can estimate their dimensions from the following considerations. In the vertical direction the dimension must be less than the scale height of the disk, 0.0003 pc. In the transverse direction the dimension is set by the linewidth of 1 km·s^{-1}, which limits the width, ΔR, to ≈0.0004 pc, from the gradient in Keplerian velocity. Because the disk is inclined to the line of sight by 7°, so that the beam angle of the masers must be greater than ≈7° for the beam to intercept the earth, the line-of-sight dimension L is limited to eight times the cross section, or 0.0025 pc (the length is also limited to about the same value by the velocity gradient along the line of sight). Hence, the volume, $V = \Delta RHL$, is $<10^{46}$ cm^3. The luminosity ($\mathcal{L}$) and flux density (F_ν) of a saturated maser is given by (e.g., ref. 31)

$$\mathcal{L} = h\nu\Delta PV, \qquad [14]$$

and

$$F_\nu = \frac{1}{2} h\nu \frac{\Delta P}{\Delta\nu} \frac{L^3}{D^2}, \qquad [15]$$

where ΔP is the differential pump rate. For a molecular density of 10^{10} cm^{-3}, a fractional water vapor abundance of 10^{-5} and a pump efficiency of 1% (e.g., ref. 31), ΔP is limited to 10^3 s^{-1}. This gives a luminosity of 1.2×10^{34} erg s^{-1} and a flux density at the earth of 10^3 Jansky (Jy). Because the high-velocity features are all <1 Jy, the volume deduced from the linewidth and beam angle is easily sufficient to produce the observed emission, provided the requisite pump source is available.

The Host Galaxy

NGC4258 is a prominent nearby spiral galaxy that has attracted a lot of attention because of some unusual characteristics. It was a late addition to the Messier catalog (M106). It is also one of the original 12 galaxies in Seyfert's catalog (32) that exhibited highly excited nuclear emission lines. More recently its nucleus has been classified as a low intensity nuclear emission region (LINER) (33). Many x-ray sources have been identified throughout the galaxy by Pietsch *et al.* (34), and a compact nuclear hard x-ray source of 4×10^{40} erg s^{-1} (2–10 keV) has been found by Makishima *et al.* (25). The spectral index and estimated column density are consistent with heavy obscuration of an active nucleus, as might be expected for the edge-on orientation of the central disk of molecular gas. There may be adequate accretion to explain the x-ray luminosity, as described above. In addition, there are anomalous spiral arms in the galactic disk that are seen in radio synchrotron emission and nonstellar H-α light and which are displaced from the stellar spiral arms. These arms are related to a bipolar jet that emerges from the nucleus at the same position angle as the spin axis of the molecular disk (35). This axis is inclined by 119° to the spin axis of the galaxy. The jet also exhibits a twisted morphology (36) whose sense, assuming outflow, agrees with the sense of rotation of the molecular disk. Both counter-rotate with respect to the galactic disk.

Future Prospects

In Table 1 we list the 15 known water megamasers, as well as the five nearby galaxies with maser emission that is probably related to star formation (e.g., in their spiral arms). The 15 megamasers come from a list of at least 250 galaxies searched in the last 12 years. So far, NGC4258 is the only megamaser known to have high-velocity satellite emission. Hence, we may have been extraordinarily lucky to have identified the one galaxy with the requisite condition to clearly reveal a nuclear disk. VLBI observations cannot be easily performed on many of the objects in Table 1 because a reference feature must be detected within the coherence time of the interferometer,

Table 1. Extragalactic H_2O masers

	D, Mpc	F_ν, Jy	α_{1950}	δ_{1950}	Ref.
Spiral arms					
LMC/SMC (7)	0.06	20	$01^h\,05^m$	−70°	37–40
M33 (5)	0.7	2	$1^h\,30^m$	30°	6, 41
IC10 (2)	1.2	30	$00^h\,17^m$	59°	42–44
NGC253	2.8	0.1	$00^h\,45^m$	−26°	45, 46
IC342 (2)	2.9	0.3	$03^h\,42^m$	68°	47
Galactic nuclei					
NGC5194 (M51)	3	0.2	$13^h\,28^m$	47°	45, 46
M82	3.5	0.2	$09^h\,51^m$	70°	5, 48
NGC4258 (M106)	6.4	4	$12^h\,16^m$	47°	5, 9, 10
NGC4945	7	4	$13^h\,02^m$	−49°	1
Circinus	7	4	$14^h\,09^m$	−65°	2
NGC1386	12	0.9	$03^h\,34^m$	−36°	49
NGC3079	16	6	$09^h\,58^m$	56°	3, 4, 7
NGC1068 (M77)	16	0.6	$02^h\,40^m$	0°	5, 10
NGC1052	20	0.3	$02^h\,38^m$	−8°	50
NGC5506	24	0.6	$14^h\,10^m$	−3°	50
IC2560	38	0.4	$10^h\,14^m$	−33°	49
NGC2639	44	0.1	$08^h\,40^m$	50°	50
ESO103-G35	53	0.7	$18^h\,33^m$	−65°	49
Mrk 1210	54	0.2	$08^h\,01^m$	5°	50
Mrk 1	65	0.1	$01^h\,13^m$	33°	50

Masers in the first group of galaxies lie in spiral arms (the number of masers are given in parentheses after the names); the second group of masers are in the galactic nuclei.

which is ≈100 sec because of fluctuations in atmospheric water vapor. This threshold condition currently limits investigations to sources stronger than ≈0.5 Jy.

The properties of the disk in NGC4258 need to be characterize more fully. The expected proper motions caused by the rotation of the disk are 32 × (6.4 Mpc/D) μas/yr. If the motions of individual features can be tracked, they will be measurable in <1 year and will allow a precise determination of the distance to be made. We have already estimated the distance to be 6.4 ± 0.9 Mpc from a comparison of the centripetal accelerations and the angular diameter of the disk. These errors are totally dominated by the uncertainty in the centripetal acceleration. It will also be possible to measure accelerations from the proper motions, which will greatly help the analysis because the masers are distributed so sparsely in the disk. Another task will be to search for a compact nuclear radio source, which we expect to have a diameter of 0.5 mas if it covers the systemic maser features, through long integration with the maser as a phase reference, to see what role it plays in the maser amplification process.

OH Megamasers

OH megamasers also offer great promise as probes of active galactic nuclei. About 50 OH megamasers have been identified (51). Their luminosities seem to be proportional to the square of the infrared luminosity of the host galaxy. This correlation is generally interpreted as an indication that the masers are unsaturated and amplify nuclear radio sources that are proportional in strength to the infrared luminosity and that the pump rate is also proportional to the infrared luminosity. The most distant examples are in the galaxies IRAS120100−4156 (z = 0.13; ref. 52) and IRAS14070+0525 (z = 0.27; ref. 53), which have luminosities of ≈10^4 solar luminosity. The original model for OH megamasers, based on low angular resolution observations of the prototypical example in the galaxy Arp 220 (IC4553), was that the maser emission arose in the extended interstellar medium of the host galaxy (54, 55). Recent VLBI observations by Lonsdale *et al.* (56) showed that the angular sizes of the OH components are small (<1 pc). Hence, OH megamasers may be much more like H_2O megamasers than originally thought (57). OH megamasers may be detectable at distances as great as 500 Mpc. However, the maximum resolution of earth-bound interferometers is ≈15 mas (a factor of 14 poorer than for H_2O megamasers). However, in one galaxy, III Zw 35, interferometric observations with MERLIN by Montgomery and Cohen (58) show some evidence for a rotating disk structure.

We thank R. Blandford, R. Booth, J. Cannizzo, W. Lewin, E. Maoz, D. Neufeld, and W. Watson for interesting discussions.

1. dos Santos, P. M. & Lepine, J. R. D. (1979) *Nature (London)* **278,** 34–35.
2. Gardner, F. F. & Whiteoak, J. B. (1982) *Mon. Not. R. Astron. Soc.* **201,** 13p–15p.
3. Henkel, C., Gusten, R., Downes, D., Thum, C., Wilson, T. L. & Biermann, P. (1984) *Astron. Astrophys.* **141,** L1–L3.
4. Haschick, A. D. & Baan, W. A. (1985) *Nature (London)* **314,** 144–146.
5. Claussen, M. J., Heiligman, G. M. & Lo, K. Y. (1984) *Nature (London)* **310,** 298–300.
6. Churchwell, E., Witzel, A., Huchtmeier, W., Pauliny-Toth, I., Roland, J. & Sieber, W. (1977) *Astron. Astrophys.* **54,** 969–971.
7. Haschick, A. D., Baan, W. A., Schneps, M. H., Reid, M. J., Moran, J. M. & Gusten, R. (1990) *Astrophys. J.* **356,** 149–155.
8. Claussen, M. J., Reid, M. J., Lo, K. Y., Moran, J. M. & Gusten, R. (1988) in *The Impact of VLBI on Astrophysics and Geophysics*, ed. Reid, M. J. & Moran, J. M. (Kluwer, Dordrecht, The Netherlands), pp. 231–232.
9. Miyoshi, M., Moran, J., Herrnstein, J., Nakai, N., Diamond, P. & Inoue, M. (1995) *Nature (London)* **373,** 127–129.
10. Claussen, M. J. & Lo, K. Y. (1986) *Astrophys. J.* **308,** 592–599.
11. Antonucci, R. R. J. & Miller, J. S. (1985) *Astrophys. J.* **297,** 621–632.
12. Greenhill, L. J., Jiang, D. R., Moran, J. M., Reid, M. J., Lo, K. Y. & Claussen, M. J. (1995) *Astrophys. J.* **440,** 619–627.
13. Nakai, N., Inoue, M. & Miyoshi, M. (1993) *Nature (London)* **361,** 45–47.
14. Watson, W. D. & Wallin, B. K. (1994) *Astrophys. J.* **432,** L35–L38.
15. Deguchi, S. (1994) *Astrophys. J.* **420,** 551–557.
16. Haschick, A. D., Baan, W. A. & Peng, E. W. (1994) *Astrophys. J. Lett.* **437,** L35–L38.
17. Greenhill, L. J., Henkel, C., Becker, R., Wilson, T. L. & Wouterloot, J. G. A. (1995) *Astron. Astrophys.*, in press.
18. Baan, W. A., Haschick, A. D. & Peng, E. W. (1993) *Bull. Am. Astron. Soc.* **25,** 1325.
19. Moran, J. M. (1993) in *Sub-Arcsecond Radio Astronomy*, eds. Davis, R. J. & Booth, R. S. (Cambridge Univ. Press, Cambridge, U.K.), pp. 62–67.
20. Weinberg, S. (1972) *Gravitation and Cosmology* (Wiley, New York), p. 188.
21. Frank, J., King, A. & Raine, D. (1992) *Accretion Power in Astrophysics* (Cambridge Univ. Press, Cambridge, U.K.).
22. Binney, J. & Tremaine, S. (1987) *Galactic Dynamics* (Princeton Univ. Press, Princeton), p. 363.
23. Maoz, E. (1995) *Astrophys. J. Lett.*, in press.
24. Neufeld, D. & Maloney, P. R. (1995) *Astrophys. J. Lett.* **447,** L17–L19.
25. Makishima, K., Fujimoto, R., Ishisaki, Y., Kii, T., Lowenstein, M., Mushotzky, R., Serlemitsos, P., Sonobe, T., Tashiro, M. & Yaqoob, T. (1994) *Proc. Astron. Soc. Jpn.* **46,** L77–L80.
26. Maoz, E. (1995) *Astrophys. J. Lett.* **447,** L91–L94.
27. Kormendy, J. & Richstone, D. (1995) *Annu. Rev. Astron. Astrophys.* **33,** 581–624.
28. Ruffini, R. & Stella, L. (1980) *Phys. Lett. B* **93,** 107–110.
29. Schandl, S. & Meyer, F. (1994) *Astron. Astrophys.* **289,** 149–161.
30. Neufeld, D., Maloney, P. R. & Conger, S. (1995) *Astrophys. J.* **436,** L127–L130.
31. Moran, J. M. (1990) in *Molecular Astrophysics*, ed. Harquist, T. W. (Cambridge Univ. Press, Cambridge, U.K.), pp. 397–423.
32. Seyfert, C. (1943) *Astrophys. J.* **97,** 28–40.
33. Heckman, T. M. (1980) *Astron. Astrophys.* **87,** 152–164.
34. Pietsch, W., Vogler, A., Kahabka, P., Jain, A. & Klein, U. (1994) *Astron. Astrophys.* **284,** 386–402.
35. Cecil, G., Wilson, A. S. & De Pree, C. (1995) *Astrophys. J.* **440,** 181–190.
36. Cecil, G., Wilson, A. S. & Tully, R. B. (1992) *Astrophys. J.* **390,** 365.
37. Whiteoak, J. B., Wellington, K. J., Jauncey, D. L., Gardner, F. F., Forster, J. R., Caswell, J. L. & Batchelor, R. A. (1983) *Mon. Not. R. Astron. Soc.* **205,** 275–279.
38. Scalise, E. & Braz, M. A. (1982) *Astron. J.* **87,** 528–531.
39. Scalise, E. & Braz, M. A. (1979) *Nature (London)* **290,** 36.
40. Whiteoak, J. B. & Gardner, F. F. (1986) *Mon. Not. R. Astron. Soc.* **222,** 513–523.
41. Huchtmeier, W. K., Eckhart, A. & Zensus, J. A. (1988) *Astron. Astrophys.* **200,** 26–28.
42. Becker, R., Henkel, C., Wilson, T. L. & Wouterloot, J. G. A. (1993) *Astron. Astrophys.* **268,** 483–490.
43. Henkel, C., Wouterloot, J. G. A. & Bally, J. (1986) *Astron. Astrophys.* **155,** 193–199.
44. Argon, A. L., Greenhill, L. J., Moran, J. M., Reid, M. J., Menten, K. M., Henkel, C. & Inoue, M. (1994) *Astrophys. J.* **422,** 586–596.
45. Ho, P. T. P., Martin, R. N., Henkel, C. & Turner, J. L. (1987) *Astrophys. J.* **320,** 663–666.
46. Nakai, N. & Kasuga, T. (1988) *Proc. Astron. Soc. Jpn.* **40,** 139–145.
47. Huchtmeier, W. K., Witzel, A., Kuhr, H., Pauliny-Toth, I. I. & Roland, J. (1978) *Astron. Astrophys.* **64,** L21–L24.
48. Baudry, A., Brouillet, N. & Henkel, C. (1995) *Astron. Astrophys.* **287,** 20–31.
49. Braatz, J. A., Wilson, A. S. & Henkel, C. (1994) *Bull. Am. Astron. Soc.* **26,** 1342.
50. Braatz, J. A., Wilson, A. S. & Henkel, C. (1994) *Astrophys. J.* **437,** L99–L102.
51. Baan, W. (1993) in *Subarcsecond Radio Astronomy*, eds. Davis, R. J. & Booth, R. S. (Cambridge Univ. Press, Cambridge, U.K.), pp. 324–330.
52. Staveley-Smith, L., Allen, D. A., Chapman, J. M., Norris, R. P. & Whiteoak, J. B. (1989) *Nature (London)* **337,** 625–627.
53. Baan, W. A., Rhoads, J., Fisher, K., Altschuler, D. R. & Haschick, A. (1992) *Astrophys. J. Lett.* **396,** L99–L102.
54. Baan, W. A. & Haschick, A. D. (1984) *Astrophys. J.* **279,** 541–549.
55. Henkel, C. & Wilson, T. L. (1990) *Astron. Astrophys.* **229,** 431–440.
56. Lonsdale, C. J., Diamond, P. J., Smith, H. E. & Lonsdale, C. J. (1995) *Nature (London)* **370,** 117–120.
57. Moran, J. M. (1995) *Nature (London)* **117,** 98–99.
58. Montgomery, A. S. & Cohen, R. J. (1992) *Mon. Not. R. Astron. Soc.* **254,** 23–26.